

Dynamic Interchange Between Two Protonation States is Characteristic of Active Sites of Cholinesterases

Alexander Zlobin^{1,2,*}, Ivan Smirnov³, Andrey Golovin^{2,3*}

1. Institute for Drug Discovery, Leipzig University, Leipzig, Germany
2. Faculty of Bioengineering and Bioinformatics, Lomonosov Moscow State University, Moscow, Russia
3. Shemyakin and Ovchinnikov Institute of Bioorganic Chemistry, Russian Academy of Sciences, Moscow, Russia

* correspondence: aleksandr.zlobin@medizin.uni-leipzig.de, golovin@fbb.msu.ru

Abstract

Cholinesterases are well-known and widely studied enzymes crucial to human health and involved in neurology, Alzheimer, and lipid metabolism. The protonation pattern of cholinesterases' active sites influences all the chemical processes within, including reaction, covalent inhibition by nerve agents, and reactivation. Our understanding of it is, however, limited. In this study, we used enhanced-sampling quantum-mechanical/molecular-mechanical calculations to show that cholinesterases mostly function as dynamical mixtures of two protonation states. Proton transfer between two non-catalytic glutamate residues occurs by Grotthuss mechanism via a mediator water molecule. We show that this uncovered complexity of active sites presents a challenge for classical molecular dynamics simulations that calls for special treatment. The proton transfer barrier of 1.65 kcal/mol opens the discussion on potential existence of two conjugated low barrier hydrogen bonds in the inhibited form of butyrylcholinesterase. These findings expand our understanding of structural features expressed by highly evolved enzymes and guide future advances in cholinesterase-related protein- and drug design studies.

Introduction

Cholinesterases – acetylcholinesterase, AChE, and butyrylcholinesterase, BChE, – attract the attention of the scientific community due to their importance for human health.¹ Some features also make them interesting for fundamental enzymology. For instance, AChE is sometimes considered to be the pinnacle of enzyme evolution with catalytic rates approaching the diffusion limit. The degradation of acetylcholine to acetic acid and choline by this enzyme is the primary mechanism for controlling the intensity of neuromuscular impulse transmission. Loss of such regulation leads to catastrophic consequences, up to lethal, which explains the choice of hAChE (human AChE) as a target for irreversible covalent inhibition by organophosphate (OP) chemical warfare agents.²

It is still debated what is the main function of hBChE. This enzyme was reported to be involved in lipid metabolism including the ability to hydrolyze the hunger hormone ghrelin.³ Reversible non-covalent inhibition of hBChE by small molecules is thought to be a path to treat Alzheimer's disease, each year witnessing hundreds of papers with suggested drug candidates.⁴ The broad binding site of hBChE, while not making it easier to pin down the "main" physiological substrate, allows for repurposing it for desired molecules by design. This way, a family of cocaine hydrolases emerged.⁵

High similarity between two enzymes allows for the use of hBChE as a suicide agent protecting against OPs. G117H variant, its derivatives and some other variants even showed the OPase activity by slowly reactivating after covalent inhibition.⁶ The mechanism of this activity remains a matter of debate, which is at least partially powered by the

lack of consensus on the number and location of hydrogen atoms on titratable residues within and around the active site.⁷

Cholinesterases are serine triad hydrolases, with the triad composed by Ser, His and Glu residues. The triad is supported by an extensive network of hydrogen bonds reaching well beyond the first interaction shell of these three residues (Figure 1). We will refer to this set of hydrogen-bonded residues as an *extended active site*. Within this region, hAChE and hBChE feature two additional glutamate residues in close vicinity to the catalytic one. On numerous occasions it was pointed out that the simultaneous existence of all three glutamates in anionic form is highly unlikely.⁷⁻¹⁰ Nevertheless, molecular modeling and computational drug design efforts sometimes continue to model a trianionic extended active site despite introducing severe artifacts.¹¹ In static docking studies or single-point quantum-mechanical/molecular-mechanical (QM/MM) calculations these artifacts are represented by an incorrect electrostatic field in the relevant region. In dynamics, electrostatic repulsion and unsaturated h-bonding networks manifest in distorted conformational ensembles. Experimental studies suggested that cholinesterases exhibit variations in flexibility with potential "breathing" motions and loop rearrangements^{12,13} affected by binding ligands and covalent inhibition. Zooming on this behavior with classical molecular dynamics (MD) is intriguing, but requires long-scale simulations that would be instantly invalidated by incorrect composition of the (extended) active site.

The latest advancements on the subject were presented in 2018 by Luschchekina and Masson.⁷ The researchers conclude that at least one excess proton should be present in the extended active site, and this proton could potentially shuttle between Glu197 and Glu441. Here we show that for classical molecular dynamics (MD) the consideration of this proton is still not enough to achieve adequate results. Untangling

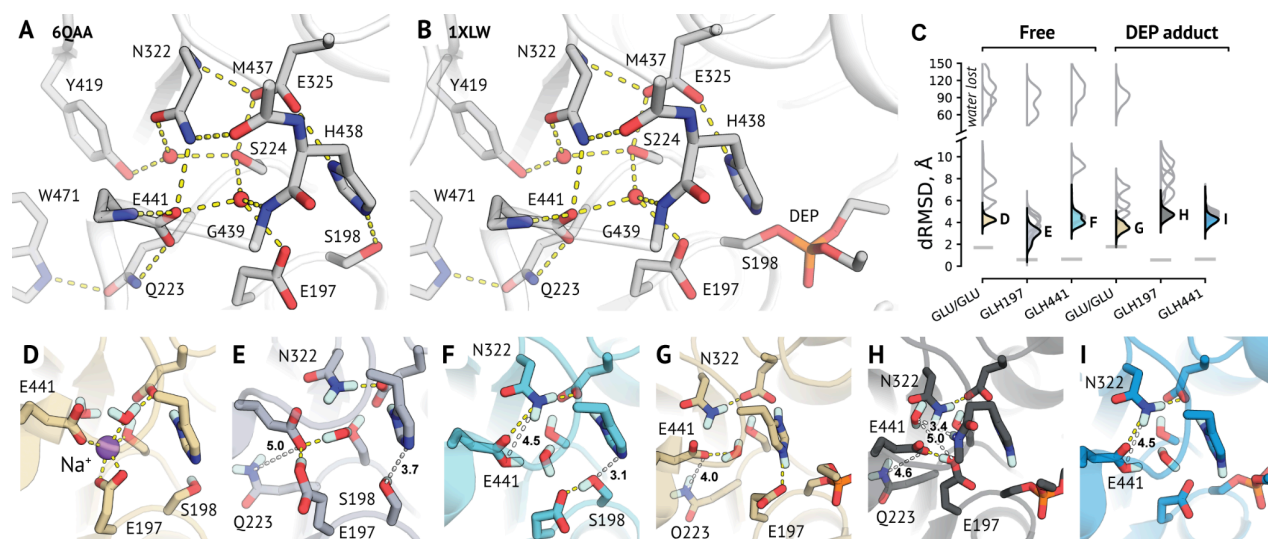


Figure 1. Reference and distorted geometries of hBChE extended active site. **A.** Reference geometry and h-bonding network for the not covalently inhibited form (PDB ID 6QAA). **B.** Reference geometry and h-bonding network for the OP-inhibited form (PDB ID 1XLW). **C.** dRMSD values for h-bonding networks after 100 ns MD simulations. For time series, refer to Figures S1,2. Gray lines represent comparison statistics obtained under position restraints. **D-I.** Snapshots of best replicas from MD simulations. Labeled are residues that moved the most. **D-F.** Free form. **G-I.** DEP-inhibited form. **D, G.** Glu197/Glu441 systems. **E, H.** Glh197/Glu441 systems. **F, I.** Glu197/Glh441 systems. White dashes represent selected lost contacts. Non-polar hydrogens are omitted for clarity.

the issue, we build upon the results of Luschekina and Masson in multiple directions. We affirm their findings in a dynamical modeling regime with QM/MM MD applied to each and every potential protonation pattern of OP-inhibited BChE extended active site. We then extend the finding to hAChE to present an extensive comparative study. We show how the balance between protonation states depends on the stage of the reaction or inhibition and how it differs between hBChE and hAChE. A crucial role of the position 322 (311 in hAChE) in this process is explained. Barriers of proton transfer in some cases vouch for the existence of a pair of conjugated low-barrier hydrogen bonds (LBHBs), a unique feature that has not been previously reported for any protein. Therefore, cholinesterases feature a unique structure of their extended active site, which is hard to reproduce in classical MD, and we conclude our work by advocating for the development of *ad hoc* restraint schemes for such studies.

Results

hBChE Active Site Breaks in Classical MD Irrespective of Protonation

A common assumption is that x-ray structures represent at least some stable conformations from those populating real ensembles. We hypothesized that the comparison of MD trajectories originating from different candidate models to the x-ray reference would allow us to establish the correct one. Our models represented three most commonly applied protonation states of the hBChE extended active site: Glu197 and Glu441 could both be without protons, or one of them harboring one proton. Additionally, we modeled hBChE as both free and covalently inhibited by an OP. The latter results in the diethyl-phosphorylated hBChE (DEP-hBChE).

No starting model was able to sustain the initial geometry (Figure 1A-C). Only free BChE with protonated Glu197 (from now on *Glh*) and DEP-hBChE with Glh441 showed mostly converging behavior (Figure S1). In both cases, the stable conformation was substantially different from the x-ray reference. A recurring feature was Asn322 losing its h-bond to the backbone oxygen of Met437 and switching to interact with the catalytic Glu325. If Glu441 were to harbor a proton, it would be bound to the upper oxygen of the carboxylate group as can be clearly seen from the electron density (Figure 2B). However, in dynamics Glh441 always flipped (Figure 1F, I). Glh197 in corresponding models switched to h-bond Glu441 directly.

Our results did not allow for drawing any conclusions on protonation states. The reason for that may be two-fold: either the initial selection of systems is incorrect, or the mechanical force field used (99SB-ildn) is incapable of correctly modeling them. It could also be true for any mechanical force field. To streamline our experimental design, we chose to systematically revisit *all* possible protonation states. To avoid potentially pointless sampling of force fields, we decided to use hybrid quantum mechanical/molecular mechanical (QM/MM) calculations.

Systematic QM/MM Study Reveals a Dynamical Balance of States

We chose to work on the DEP-BChE system, from which the answer, once obtained, may be extended onto all other states. We performed enhanced-sampling QM/MM MD simulations, allowing protons to move freely within h-bonding networks we called “proton depots” (Figure 2C). All possible protonation states can be divided into groups that share the same amount of protons in both depots. Such a setup allowed us to study these states systematically. For each such group, we then modeled proton rearrangements in dynamics. We kept the positions of all protein heavy atoms close to the reference, thus biasing the whole protocol to output *the probabilities of locations of protons given their number and a particular active site geometry*. We note that due to these restraints, the absolute energy values in this setup are not directly interpretable, and we are interested only in relative energy differences between end states. Given the scale of the experiment, for the QM part we chose a fast semiempirical DFTB3 method that was previously shown to give reasonable results for biochemical systems.^{14,15}

Each depot may realistically hold from 0 to 2 protons. More than 2 protons start to violate the saturation of h-bonding networks, while 0 protons could mean undersaturation. States within these 9 groups differ by exact locations of protons. To be able to model and distinguish them, we designed unique sets of collective variables (Figure 2C, 3). For example, groups with no protons in depot 1 are all undersaturated, and the water molecule (HOH1117 in 1XLW, Fig2A) may freely choose its two interacting partners from three possible (Fig3, A-C). All relevant states were distinguishable with up to two tailored variables.

By analyzing the resulting free energy profiles for each group, we extract one or more candidate states for further all-vs-all comparison (Figure 3). We did not take any minima that was more than 5 kcal/mol

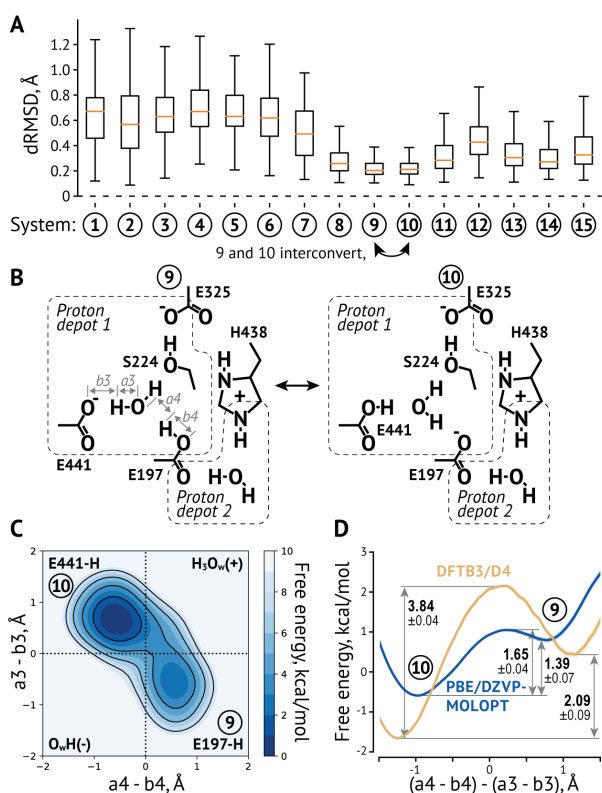


Figure 4. Identification of the protonation state of DEP-hBChE. **A.** Retention of the reference active site structure in QM/MM MD for all selected systems. **B.** Schemes of systems 9 and 10 that populate the correct DEP-hBChE ensemble. **C.** 2-d free energy profile of the proton transfer, DFTB3/MM. **D.** Comparison of DFTB3-D4/MM and PBE/DZVP-MOLOPT free energy profiles. Shaded areas represent standard error of means.

In hAChE, the balance of states is generally shifted more to the protonated *external* Glu202 (hBChE: Glu197) (Figure 5A). The only hAChE state that prefers a protonated *internal* Glu450 (hBChE: Glu441) is the covalently inhibited one, much like the DEP-hBChE. This state, alongside with the pre-reaction complex (ES) and both tetrahedral intermediates (TI1 and TI2), still feature a dynamic interconversion between both protonation variants. However, the free enzyme state, the acyl-enzyme, and the final product state (EP) have a proton almost exclusively on their external Glu.

All hBChE states along the normal reaction retain the dynamical proton transfer. In the free form, the Michaelis complex, and the TI1 state, it is equally likely to have a proton on either external or internal Glu. The EP state shows a preference for the protonated external Glu, while it is the other way around for the TI2 and the acyl-enzyme. In contrast, binding of OP inhibitors echothiophate and soman abolish the possibility of observing the protonated internal Glu.

Structures of hAChE and hBChE Extended Active Sites Explain Differences in the Protonation State Balance

Human cholinesterases demonstrated markedly different behavior. The only difference in the structure of the extended active site is the identity of the residue 331 (hAChE) or 322 (hBChE) (Figure 5C, D). Asn322 in hBChE directly interacts with Glu441, while the more buried water molecule of the pair (HOH1109 in 1XLW) does not, instead also forming an h-bond with Asn322. This results in the upper oxygen of Glu441 forming three h-bonds, and the lower one only one (Figure 5C, h-bond to HOH1117 not shown). hAChE, in contrast, has Val331 in place of Asn. The buried water molecule switches to interact with Glu450, and it forms two h-bonds with each of its oxygens (Figure 5D).

This influences the rotation of the carboxylate group and the basicity of its individual oxygens.

Other factors may also be at play here, for instance the overall electrostatic field or subtle differences in the architecture. hBChE is slightly more similar to AChE from *Torpedo californica* than to hAChE (72% vs 69% sequence similarity), and tcAChE also harbors Asn in the position in question (Fig 5E). To quantify the role of position 331/322, we extended the analysis onto tcAChE and performed *in silico* mutagenesis to the opposite amino acid for all three cholinesterases. We found a consistent trend of the N>V substitution lowering the basicity of the internal Glu, and the V>N substitution raising it (Fig 5B).

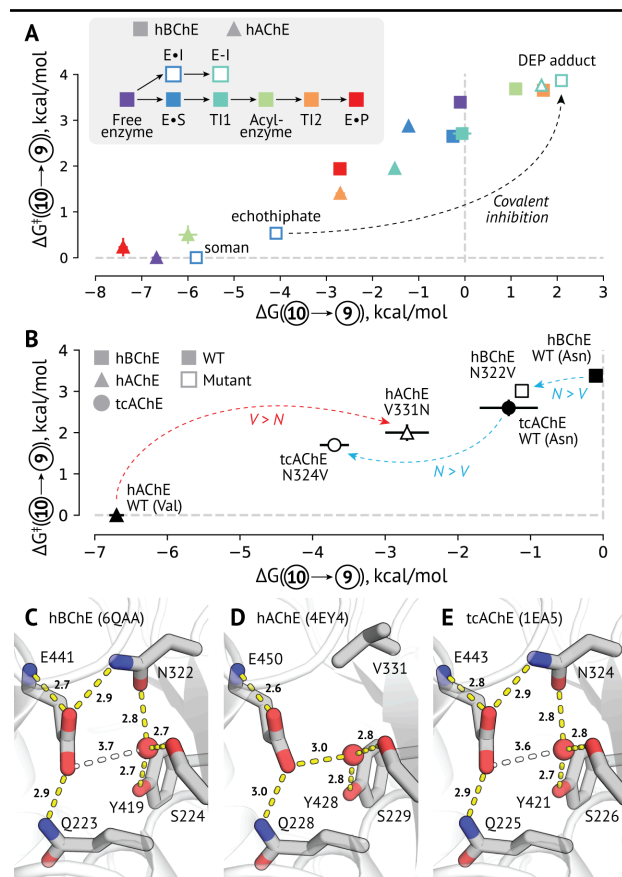


Figure 5. Preferences for Glu197 or Glu441 differ between hAChE and hBChE, in reaction and inhibition stages and with the substitution of the key active site residue. **A.** Free energy differences and barriers for the proton transfer in stable states along the reaction and inhibition processes. The X axis below 0 indicates the preference for Glu197. **B.** Differences in the proton hopping behavior of WT and mutated hAChE, hBChE and tcAChE in the free form. Reciprocal N↔V substitutions soften the differences between the enzymes. Error bars represent standard error of means, some bars are smaller than markers. Exact values can be found in Table S1, profiles in Figures S14-17. **C-E.** Differences in the internal Glu interactions in three cholinesterases. **C.** hBChE. **D.** hAChE. **E.** tcAChE. White dashes represent the absence of the interaction.

Discussion

X-ray Structures May Introduce Biases

In this study, we heavily relied on x-ray structures as references for the extended active site geometry. Some calculations directly used positional restraints. The bias that originates with the limitations in resolution and inaccuracies of refinement is propagated to MD. Furthermore, hBChE entry 1P0I that is commonly used for molecular replacement – even for presumably unliganded forms – features a chemically modified catalytic serine.¹⁶ This model itself used phases from 2ACE, a tcAChE structure also harboring a modified Ser residue.¹⁷

hAChE models are also traced down to tcAChE model IFSS.¹⁸ Therefore, there may be less similarities between free and ligand-bound forms and between hAChE and hBChE that are currently observable in PDB. Further advancements in purification and Cryo-EM may present new insights into the structures of cholinesterases that will help rectify the results obtained herein.

A Pair of Conjugated Low-Barrier Hydrogen Bonds May Be Present in Cholinesterases

LBHBs are a special case of hydrogen bonds formed between polar atoms with comparable pKa values and characterized by delocalization of a proton that becomes equally shared.¹⁹ The existence of LBHBs in proteins is debated. Neutron crystallography is able to unambiguously reveal such interactions within protein structures.²⁰ Despite progress,²¹ no such structures are currently available for cholinesterases. Most predictions on LBHBs come from Born-Oppenheimer QM/MM calculations. Such calculations are incapable of modeling proton tunneling and are believed to provide heightened proton transfer barriers. Taking into account these limitations, researchers suggest that computed barriers of <2 kcal/mol may hint on potential LBHBs.^{20,22,23} In this study, for the concerted transfer of two protons we obtained the PBE estimate of the barrier of 1.65 kcal/mol (Figure 4D). Therefore, there may be a possibility that cholinesterases harbor a conjugated pair of two LBHBs, a structural unit never reported for proteins before. Further studies, both experimental and computational – with larger QM regions,²⁴ polarizable embeddings,²⁵ and accounting for nuclear quantum effects²⁶ – are needed to scrutinize this hypothesis. Some structurally similar enzymes feature even more titratable residues in their extended active sites (Figure S18), which may add further complexity to the issue.

Proton Transfer May Accompany the Reaction

Some of the biggest changes in the balance of protonation states that we uncovered correspond to subsequent stages in the reaction or inhibition processes. They include the inhibition of hBChE by OP echthiophate and the first chemical stage of hAChE reaction with its substrate (Figure 5A). While the protonation balance may shift as the result of the protein adjusting to a new state, this shift may also be a part of the reaction itself. Whether it is true, and what role this coupling of the reaction to the proton transfer may have, remain open questions. In this context it is intriguing to add E197Q hBChE into consideration. This variant obviously loses the proton transfer feature and demonstrates 11-fold drop in activity towards butyrylcholine.²⁷

Ad hoc Restraints May Be Needed to Study Cholinesterases with Classical MD

In the beginning of this work, we showed that we are unable to correctly model hBChE, both free and DEP-inhibited, via classical MD. This notion corresponds well with our results on the delocalized nature of the proton in both these states. On the other hand, free hAChE is exclusively in Glh202 state. We modeled the dynamics of hAChE and 9 other structurally related enzymes with the external Glu protonated. No inter-replica convergence was observed for any of these enzymes (Figure S19-28). However, the best replica for hAChE demonstrated a conformation quite close to the reference (Figure S25). It seems likely that systems with less pronounced proton delocalization are easier to model correctly with classical MD. For other systems, *ad hoc* restraints may be needed to prevent the incorrect modeling of the active site. While concrete realization of such is to be devised, for hBChE we suggest that targeting non-bonded interactions between the water molecule and Glu197, Glu441 and Ser224 may be crucial (Figure 6).

Once the practical ability of using classical MD to model hBChE is established, some intriguing directions may be pursued. Previously we suggested that conformational rearrangements of the acyl-binding loop explain the OPase activity of c114 and c115 variants.²⁸ Quantitative evaluation of this idea with MD treatment may be beneficial in general

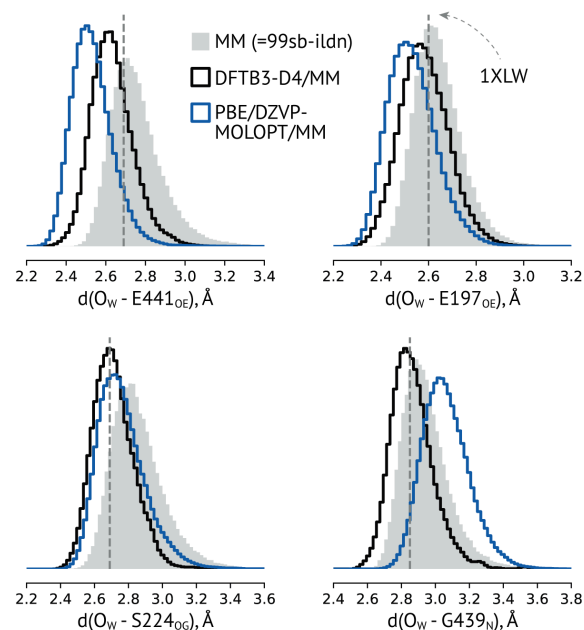


Figure 6. Differences in the water-binding geometry of the DEP-hBChE active site under different treatment. For 99SB-ildn, the Glh441 system was used. Gray dash represents measurements from the 1XLW x-ray structure.

and instrumental for other similar cases that recently emerged.²⁹ Our results on the protonation prompt to re-evaluate possibilities for various proposed mechanisms of G117H action⁷ that may potentially include minor conformations, unseen in x-ray, being the reactive ones.^{10,30} Being able to obtain ensembles of conformations also dramatically raises the possibilities of modern computational protein design approaches³¹⁻³³ that may help to create a better OPase hBChE variant.

Conclusions

The exact protonation state of cholinesterase active sites remained a puzzle hampering further progress in understanding their structure-function relationships and applied enzyme design studies. In this paper, we systematically explored all possibilities for the number and location of protons within the active site of covalently inhibited hBChE. We established that the balance of two states is typical for this state. A proton may be either on the internal (441) or external (197) Glu residue, and the interconversion is mediated by the water molecule by the Grothuss mechanism. The same was found true for most of the stages hBChE passes along the native reaction process. In contrast, collapse to mostly one state is a more typical, albeit not only, scenario for hAChE. We compared proton transfer dynamics in hAChE, tcAChE and hBChE, and highlighted the crucial role of the residue Val331 (Asn324, Asn322) in the observed differences. The free energy profile calculated for the inhibited hBChE form on the PBE level suggests a constant dynamical rearrangement of protons or even a system of two conjugated LBHBs. This fine structure of cholinesterase active sites is hard to model correctly with classical MD, therefore we suggest the need of developing *ad hoc* force field corrections. Our findings generally advance cholinesterase studies and delineate a particularly complex case relevant for the broader field of fundamental enzymology.

Materials and Methods

Simulation Software

All simulations were performed with Gromacs.³⁴ For MM simulations we used Gromacs 2021.3 and 2023.1. For QM/MM simulations with DFTB3 we used an interface between Gromacs and DFTB+^{35,36} patched with Plumed 2.8.0.³⁷ For PBE level simulations, we used the internal Gromacs 2023.1 QM/MM interface to CP2K.³⁸ QM/MM calculations were carried out using the equipment of the shared research facilities of HPC computing resources at the Lomonosov Moscow State University.³⁹

System Preparation and Classical MD

Models in this study were based on several PDB entries outlined in the SI section. Models were parameterized with the Amber ff99SB-ildn⁴⁰ force field chosen based on our previous findings for enzymatic systems.⁴¹ Diethyl-phosphorylated (DEP) serine was parameterized as a single residue by combining force-field Ser parameters with ones derived for a triethyl-phosphate moiety. It was done with the **parameterize** tool by tailoring GAFF2 torsions towards QM scans on the wB97X-D level of theory with aug-cc-pVDZ basis set⁴² similarly to what was done before.⁴³ Charges were assigned with the RESP protocol. Other ligands and Ser modifications used in the study (Figure S12-13) were not used in unrestrained classical MD and thus did not require tailored parameters. For topology placeholders, they were parameterized with the GAFF2 force field with acpype with AM1-BCC charges.⁴⁴

Each system was placed in a cubic box with periodic boundary conditions and solvated with tip3p-FB.⁴⁵ All crystallographic water molecules were retained while all added were manually filtered in case of incorrect solvation. Na⁺ and Cl⁻ ions were added to neutralize the net charge and reach 0.15M ionic strength. Systems were minimized with 5000 steps of steepest descent. The equilibration phase consisted of seven steps and was performed in 5 replicates for each BChE system and in 3 replicates for others. First, an NVT run of 500 ps was performed while positionally restraining heavy atoms by 1000 kJ/mol/nm². Velocity rescale thermostat was utilized⁴⁶ for temperature coupling under 300K. Then, for five rounds of NPT equilibration of 500 ps each, restraint strength was gradually decreased as follows: 1000, 1000, 500, 200, 100 kJ/mol/nm² respectively. The NVT stage and the first NPT stage used a flexible water treatment (no LINKS constraints) for finer position adjustment. Stochastic cell-rescale barostat was used for pressure control.⁴⁷ 2 fs time step was used in all steps. The final step was an unrestrained NPT run of 100 ns.

We chose to use distance RMSD values (dRMSDs) over position RMSDs due to much higher sensitivity and since we previously defined extended active sites as predominantly h-bonding networks. dRMSD values were calculated for sets of 12-16 distances (see detailed lists in the Supplementary Information section). For hBChE systems, distributions of dRMSD values were computed for the last 5 ns of unrestrained MD run. Reference values on graphs correspond to mean values from the first NPT step.

DFTB3/MM System Preparation

Coordinates after the MM minimization step were used as starting to prevent a potential drift manifested due to the incorrect protonation and forcefield limitations. Then, 500 ps of NVT and NPT equilibration steps were performed while restraining heavy atoms including water oxygens by 100 000 kJ/mol/nm². Water was treated as flexible for finer position adjustment.

QM subsystems consisted of 217-221 atoms for hBChE-DEP scans, 173-220 for hAChE in different stages, 171-230 for hBChE in different stages, and 171-173 for the tcAChE(-NV) free form. Free forms lacked a portion of the oxyanion hole, otherwise all other stages and systems shared the same composition that differed only by the nature of the

ligand or adduct (Figure S26). To prevent link atom hyperpolarization, a “charge shifting” scheme was used. The effect of non-integer charge of the QM system on PME was alleviated with the Amber scheme as discussed before.⁴⁸ The QM region was described with DFTB3⁴⁹ with 3ob-3-1 parameter set⁵⁰ similarly to what was used before in various enzymological tasks.^{15,28,51-54} Additionally, D4 dispersion correction⁵⁵ was utilized. All reported simulations were performed with periodic boundary conditions and full PME treatment for QM/MM electrostatics.

Scans of DEP-hBChE Protonation Possibilities

Throughout this section, position restraints of 100 000 kJ/mol/nm² were applied on all protein heavy atoms to bias results to the reference 1XLW geometry. Systems were first subjected to up to 1000 steps of conjugate gradient minimization, followed by 1 ps QM/MM equilibration with 1 fs time step. Finally, production runs were performed in 3 replicates of 14 parallel walkers each. A time step of 0.5 fs was used, and each walker sampled for 50 ps. Velocity-rescale thermostat was used with no pressure control. Multiple-walkers well-tempered metadynamics was used to sample proton location possibilities and reconstruct free energy profiles.⁵⁶ Collective variables used are illustrated in Figures 2 and 3, and more detail is given in the Supplementary Information section. Metadynamics potential 1.046 kJ/mol high was applied each 100th step. Potential width was 0.25 radians for water molecule rotation and 0.2 Å for all distance-based variables. Bias factor was set to 20 except for runs only simulating water molecule rotation, in which it was 12. Free energy profiles were reconstructed with Tiwary reweighting,⁵⁷ with the first 5 ps of each walker discarded as initial transient. 15 systems corresponding to deepest local minima were selected for subsequent analysis. For that, positional restraints were lifted from the QM region, and each system was sampled for 10 ps with 0.5 fs step in 50 replicates. dRMSD values were assessed by aggregating the last 1 ps of each replica.

Proton Rearrangements in Different States

We performed 1000 steps of conjugate gradient minimization and 10 ps of QM/MM equilibration with 0.5 fs time step. Position restraints of 1000 kJ/mol/nm² were active on protein heavy atoms in the MM region only. Production time was 20 ps per walker, potential height and width were 0.5 kJ/mol and 0.1 Å respectively. Bias factor was set to 10. All other setup and analysis details were the same as above.

PBE/MM Calculations

A minimal QM system of Glu197 and Glu441 side chains with the interacting water molecule was used. Backbone charges of both Glu were averaged to avoid the potential bias of the initial state assignment. Amber2 charge compensation scheme was used. GROMACS pull code was used to put umbrella restraints on the reaction coordinate. 100 000 kJ/mol/nm² restraints were used during the initial conjugate gradient minimization and then decreased to 5 000 kJ/mol/nm² for umbrella sampling runs in 11 windows with centers in range from -1.5 Å to 1.5 Å with 0.3 Å increments. Each window was sampled for 5 ps with 1 fs time step in 100 replicates. First 0.5 ps were discarded, and subsequent data was grouped in sets of 20 runs per window to yield 5 independent profile reconstructions with the binless WHAM method. Sufficient histogram overlap was achieved for each (Figure S27). Position restraints of 100 kJ/mol/nm² were active on protein heavy atoms in the MM region only. Velocity-rescale thermostat was used with no pressure control.

Geometry of Interactions with the Water Molecule

MM statistics were collected by re-running the last (unrestrained) equilibration step of Glh441 system for 100 ps in 50 replicates. DFTB3/MM and PBE/MM values are weighted histograms from the corresponding metadynamics and umbrella sampling simulations.

Supporting Information

Following additional data is available:

- Supplementary data. **Figures:** S1. Overtime changes of dRMSD values of the extended active site h-bonding network of hBChE systems. S2. Backbone heavy atom RMSD values of hBChE systems over the course of MD. S3-S11. 15 selected hBChE-DEP systems. S12,13. Structures of ligands and adducts in individual hAChE and hBChE systems. S14-17. DFTB3-D4/MM free energy profiles for concerted proton transfer. S18. Additional titratable residues in the extended active sites in cholinesterase-related enzymes. S19-28. Dynamical stability of the reference geometry of cholinesterase-related enzymes. **Tables:** S1. DFTB3-D4/MM values for all systems extracted from the analysis of free energy profiles.
- Extended Materials and Methods section

Acknowledgements

We are grateful to Arthur Zalevsky and Julia Beliaeva for critical discussions and support.

Funding

This work was supported by Russian Science Foundation Grant 21-74-20113

References

- (1) Silman, I. The Multiple Biological Roles of the Cholinesterases. *Prog. Biophys. Mol. Biol.* **2021**, *162*, 41–56.
- (2) Poirier, L.; Jacquet, P.; Plener, L.; Masson, P.; Daudé, D.; Chabrière, E. Organophosphorus Poisoning in Animals and Enzymatic Antidotes. *Environ. Sci. Pollut. Res. Int.* **2021**, *28* (20), 25081–25106.
- (3) Furtado-Alle, L.; Tureck, L. V.; de Oliveira, C. S.; Hortega, J. V. M.; Souza, R. L. R. Butyrylcholinesterase and Lipid Metabolism: Possible Dual Role in Metabolic Disorders. *Chem. Biol. Interact.* **2023**, *383*, 110680.
- (4) Jing, L.; Wu, G.; Kang, D.; Zhou, Z.; Song, Y.; Liu, X.; Zhan, P. Contemporary Medicinal-Chemistry Strategies for the Discovery of Selective Butyrylcholinesterase Inhibitors. *Drug Discov. Today* **2019**, *24* (2), 629–635.
- (5) Ha, Z. Y.; Mathew, S.; Yeong, K. Y. Butyrylcholinesterase: A Multifaceted Pharmacological Target and Tool. *Curr. Protein Pept. Sci.* **2020**, *21* (1), 99–109.
- (6) Lushchekina, S. V.; Schopfer, L. M.; Grigorenko, B. L.; Nemukhin, A. V.; Varfolomeev, S. D.; Lockridge, O.; Masson, P. Optimization of Cholinesterase-Based Catalytic Bioscavengers Against Organophosphorus Agents. *Front. Pharmacol.* **2018**, *9*, 211.
- (7) Lushchekina, S.; Masson, P. Catalytic Bioscavengers against Organophosphorus Agents: Mechanistic Issues of Self-Reactivating Cholinesterases. *Toxicology* **2018**, *409*, 91–102.
- (8) Masson, P.; Fortier, P. L.; Albaret, C.; Froment, M. T.; Bartels, C. F.; Lockridge, O. Aging of Di-Isopropyl-Phosphorylated Human Butyrylcholinesterase. *Biochem. J* **1997**, *327* (Pt 2), 601–607.
- (9) Wan, X.; Yao, Y.; Fang, L.; Liu, J. Unexpected Protonation State of Glu197 Discovered from Simulations of Tacrine in Butyrylcholinesterase. *Phys. Chem. Chem. Phys.* **2018**, *20* (21), 14938–14946.
- (10) Amitay, M.; Shurki, A. The Structure of G117H Mutant of Butyrylcholinesterase: Nerve Agents Scavenger. *Proteins* **2009**, *77* (2), 370–377.
- (11) De Boer, D.; Nguyen, N.; Mao, J.; Moore, J.; Sorin, E. J. A Comprehensive Review of Cholinesterase Modeling and Simulation. *Biomolecules* **2021**, *11* (4). <https://doi.org/10.3390/biom11040580>.
- (12) Peters, J.; Martinez, N.; Trovaslet, M.; Scannapieco, K.; Koza, M. M.; Masson, P.; Nachon, F. Dynamics of Human Acetylcholinesterase Bound to Non-Covalent and Covalent Inhibitors Shedding Light on Changes to the Water Network Structure. *Phys. Chem. Chem. Phys.* **2016**, *18* (18), 12992–13001.
- (13) Gerlits, O.; Fajer, M.; Cheng, X.; Blumenthal, D. K.; Radić, Z.; Kovalevsky, A. Structural and Dynamic Effects of Paraoxon Binding to Human Acetylcholinesterase by X-Ray Crystallography and Inelastic Neutron Scattering. *Structure* **2022**, *30* (11), 1538–1549.e3.
- (14) Lai, R.; Cui, Q. How to Stabilize Carbenes in Enzyme Active Sites without Metal Ions. *J. Am. Chem. Soc.* **2022**, *144* (45), 20739–20751.
- (15) Roston, D.; Demapan, D.; Cui, Q. Extensive Free-Energy Simulations Identify Water as the Base in Nucleotide Addition by DNA Polymerase. *Proc. Natl. Acad. Sci. U. S. A.* **2019**, *116* (50), 25048–25056.
- (16) Nicolet, Y.; Lockridge, O.; Masson, P.; Fontecilla-Camps, J. C.; Nachon, F. Crystal Structure of Human Butyrylcholinesterase and of Its Complexes with Substrate and Products. *J. Biol. Chem.* **2003**, *278* (42), 41141–41147.
- (17) Raves, M. L.; Harel, M.; Pang, Y. P.; Silman, I.; Kozikowski, A. P.; Sussman, J. L. Structure of Acetylcholinesterase Complexed with the Nootropic Alkaloid, (-)-Huperzine A. *Nat. Struct. Biol.* **1997**, *4* (1), 57–63.
- (18) Harel, M.; Kleywegt, G. J.; Ravelli, R. B.; Silman, I.; Sussman, J. L. Crystal Structure of an Acetylcholinesterase-Fasciculin Complex: Interaction of a Three-Fingered Toxin from Snake Venom with Its Target. *Structure* **1995**, *3* (12), 1355–1366.
- (19) Kemp, M. T.; Lewandowski, E. M.; Chen, Y. Low Barrier Hydrogen Bonds in Protein Structure and Function. *Biochim. Biophys. Acta: Proteins Proteomics* **2021**, *1869* (1), 140557.
- (20) Drago, V. N.; Dajnowicz, S.; Parks, J. M.; Blakeley, M. P.; Keen, D. A.; Coquelle, N.; Weiss, K. L.; Gerlits, O.; Kovalevsky, A.; Mueser, T. C. An N-H-N Low-Barrier Hydrogen Bond Preorganizes the Catalytic Site of Aspartate Aminotransferase to Facilitate the Second Half-Reaction. *Chem. Sci.* **2022**, *13* (34), 10057–10065.
- (21) Gerlits, O.; Blakeley, M. P.; Keen, D. A.; Radić, Z.; Kovalevsky, A. Room Temperature Crystallography of Human Acetylcholinesterase Bound to a Substrate Analogue 4K-TMA: Towards a Neutron Structure. *Curr Res Struct Biol* **2021**, *3*, 206–215.
- (22) Nichols, D. A.; Hargis, J. C.; Sanishvili, R.; Jaishankar, P.; Defrees, K.; Smith, E. W.; Wang, K. K.; Prati, F.; Renslo, A. R.; Woodcock, H. L.; Chen, Y. Ligand-Induced Proton Transfer and Low-Barrier Hydrogen Bond Revealed by X-Ray Crystallography. *J. Am. Chem. Soc.* **2015**, *137* (25), 8086–8095.
- (23) Porter, M. A.; Molina, P. A. The Low-Barrier Double-Well Potential of the O(δ)(1)-H-O(δ)(1) Hydrogen Bond in Unbound HIV Protease: A QM/MM Characterization. *J. Chem. Theory Comput.* **2006**, *2* (6), 1675–1684.
- (24) Vennelakanti, V.; Nazemi, A.; Mehmood, R.; Steeves, A. H.; Kulik, H. J. Harder, Better, Faster, Stronger: Large-Scale QM and QM/MM for Predictive Modeling in Enzymes and Proteins. *Curr. Opin. Struct. Biol.* **2022**, *72*, 9–17.
- (25) Loco, D.; Lagardère, L.; Caprasecca, S.; Lippardini, F.; Mennucci, B.; Piquemal, J.-P. Hybrid QM/MM Molecular Dynamics with AMOEBA Polarizable Embedding. *J. Chem. Theory Comput.* **2017**, *13* (9), 4025–4033.
- (26) Cassone, G. Nuclear Quantum Effects Largely Influence Molecular Dissociation and Proton Transfer in Liquid Water under an Electric Field. *J. Phys. Chem. Lett.* **2020**, *11* (21), 8983–8988.
- (27) Millard, C. B.; Lockridge, O.; Broomfield, C. A. Organophosphorus Acid Anhydride Hydrolase Activity in Human Butyrylcholinesterase: Synergy Results in a Somanase. *Biochemistry* **1998**, *37* (1), 237–247.
- (28) Zlobin, A.; Mokrushina, Y.; Terekhov, S.; Zalevsky, A.; Bobik, T.; Stepanova, A.; Aliseychik, M.; Kartseva, O.; Panteleev, S.; Golovin, A.; Belogurov, A., Jr.; Gabibov, A.; Smirnov, I. QM/MM Description of Newly Selected Catalytic Bioscavengers Against Organophosphorus Compounds Revealed Reactivation Stimulus Mediated by Histidine Residue in the Acyl-Binding Loop. *Front. Pharmacol.* **2018**, *9*, 834.
- (29) Schnettler, J. D.; Klein, O. J.; Kaminski, T. S.; Colin, P.-Y.; Hollfelder, F. Ultra-high-Throughput Directed Evolution of a Metal-Free α/β -Hydrolase with a Cys-His-Asp Triad into an Efficient Phosphotriesterase. *J. Am. Chem. Soc.* **2023**, *145* (2), 1083–1096.
- (30) Amitay, M.; Shurki, A. Hydrolysis of Organophosphate Compounds by Mutant Butyrylcholinesterase: A Story of Two Histidines. *Proteins* **2011**, *79* (2), 352–364.
- (31) Sumida, K. H.; Núñez-Franco, R.; Kalvet, I.; Pellock, S. J.; Wicky, B. I. M.; Milles, L. F.; Dauparas, J.; Wang, J.; Kipnis, Y.; Jameson, N.; Kang, A.; De La Cruz, J.; Sankaran, B.; Bera, A. K.; Jiménez-Osés, G.; Baker, D. Improving Protein Expression, Stability, and Function with ProteinMPNN. *J. Am. Chem. Soc.* **2024**. <https://doi.org/10.1021/jacs.3c110941>.
- (32) Broom, A.; Rakotoharisoa, R. V.; Thompson, M. C.; Zarifi, N.; Nguyen, E.; Mukhametzhonov, N.; Liu, L.; Fraser, J. S.; Chica, R. A. Ensemble-Based Enzyme Design Can Recapitulate the Effects of Laboratory Directed Evolution in Silico. *Nat. Commun.* **2020**, *11* (1), 4808.
- (33) Crean, R. M.; Gardner, J. M.; Kamerlin, S. C. L. Harnessing Conformational Plasticity to Generate Designer Enzymes. *J. Am. Chem. Soc.* **2020**, *142* (26), 11324–11342.
- (34) Abraham, M. J.; Murtola, T.; Schulz, R.; Páll, S.; Smith, J. C.; Hess, B.; Lindahl, E. GROMACS: High Performance Molecular Simulations through Multi-Level Parallelism from Laptops to Supercomputers. *SoftwareX* **2015**, *1-2*, 19–25.
- (35) Gillet, N.; Elstner, M.; Kubař, T. Coupled-Perturbed DFTB-QM/MM Metadynamics: Application to Proton-Coupled Electron Transfer. *J. Chem. Phys.* **2018**, *149* (7), 072328.
- (36) Hourahine, B.; Aradi, B.; Blum, V.; Bonafé, F.; Buccheri, A.; Camacho, C.; Celvallos, C.; Deshayes, M. Y.; Dumitrică, T.; Dominguez, A.; Ehlert, S.; Elstner, M.; van der Heide, T.; Hermann, J.; Irle, S.; Kranz, J. J.; Köhler, C.; Kowalczyk, T.; Kubař, T.; Lee, I. S.; Lutsker, V.; Maurer, R. J.; Min, S. K.; Mitchell, I.; Negre, C.; Niehaus, T. A.; Niklasson, A. M. N.; Page, A. J.; Pecchia, A.; Penazzi, G.; Persson, M. P.; Rezáč, J.; Sánchez, C. G.; Sternberg, M.; Stöhr, M.; Stuckenberg, F.; Tkatchenko, A.; Yu, V. W.-Z.; Frauenheim, T. DFTB+, a Software Package for Efficient Approximate Density Functional Theory Based Atomistic Simulations. *J. Chem. Phys.* **2020**, *152* (12), 124101.
- (37) Bussi, G.; Tribello, G. A. Analyzing and Biasing Simulations with PLUMED. *Methods Mol. Biol.* **2019**, *2022*, 529–578.

- (38) Kühne, T. D.; Iannuzzi, M.; Del Ben, M.; Rybkin, V. V.; Seewald, P.; Stein, F.; Laino, T.; Khaliullin, R. Z.; Schütt, O.; Schiffmann, F.; Golze, D.; Wilhelm, J.; Chulkov, S.; Bani-Hashemian, M. H.; Weber, V.; Borštnik, U.; Taillefumier, M.; Jakobovits, A. S.; Lazzaro, A.; Pabst, H.; Müller, T.; Schade, R.; Guidon, M.; Andermatt, S.; Holmberg, N.; Schenter, G. K.; Hehn, A.; Bussy, A.; Belleflamme, F.; Tabacchi, G.; Glöb, A.; Lass, M.; Bethune, I.; Mundy, C. J.; Plessl, C.; Watkins, M.; VandeVondele, J.; Krack, M.; Hutter, J. CP2K: An Electronic Structure and Molecular Dynamics Software Package - Quickstep: Efficient and Accurate Electronic Structure Calculations. *J. Chem. Phys.* **2020**, *152* (19), 194103.
- (39) Supercomputer Lomonosov-2: Large Scale, Deep Monitoring and Fine Analytics for the User Community. *Supercomput. Front. Innov.* **2019**, *6* (2). <https://doi.org/10.14529/jsfi190201>.
- (40) Lindorff-Larsen, K.; Piana, S.; Palmo, K.; Maragakis, P.; Klepeis, J. L.; Dror, R. O.; Shaw, D. E. Improved Side-Chain Torsion Potentials for the Amber ff99SB Protein Force Field. *Proteins* **2010**, *78* (8), 1950–1958.
- (41) Belyaeva, J.; Zlobin, A.; Maslova, V.; Golovin, A. Modern Non-Polarizable Force Fields Diverge in Modeling the Enzyme-Substrate Complex of a Canonical Serine Protease. *Phys. Chem. Chem. Phys.* **2023**, *25* (8), 6352–6361.
- (42) Galvelis, R.; Doerr, S.; Damas, J. M.; Harvey, M. J.; De Fabritiis, G. A Scalable Molecular Force Field Parameterization Method Based on Density Functional Theory and Quantum-Level Machine Learning. *J. Chem. Inf. Model.* **2019**, *59* (8), 3485–3493.
- (43) Zlobin, A.; Diankin, I.; Pushkarev, S.; Golovin, A. Probing the Suitability of Different Ca Parameters for Long Simulations of Diisopropyl Fluorophosphatase. *Molecules* **2021**, *26* (19). <https://doi.org/10.3390/molecules26195839>.
- (44) Kagami, L.; Wilter, A.; Diaz, A.; Vranken, W. The ACPYPE Web Server for Small-Molecule MD Topology Generation. *Bioinformatics* **2023**, *39* (6). <https://doi.org/10.1093/bioinformatics/btad350>.
- (45) Izadi, S.; Onufriev, A. V. Accuracy Limit of Rigid 3-Point Water Models. *J. Chem. Phys.* **2016**, *145* (7), 074501.
- (46) Bussi, G.; Donadio, D.; Parrinello, M. Canonical Sampling through Velocity Rescaling. *J. Chem. Phys.* **2007**, *126* (1), 014101.
- (47) Bernetti, M.; Bussi, G. Pressure Control Using Stochastic Cell Rescaling. *J. Chem. Phys.* **2020**, *153* (11), 114107.
- (48) Zlobin, A.; Belyaeva, J.; Golovin, A. Challenges in Protein QM/MM Simulations with Intra-Backbone Link Atoms. *J. Chem. Inf. Model.* **2023**, *63* (2), 546–560.
- (49) Gaus, M.; Cui, Q.; Elstner, M. DFTB3: Extension of the Self-Consistent-Charge Density-Functional Tight-Binding Method (SCC-DFTB). *J. Chem. Theory Comput.* **2012**, *7* (4), 931–948.
- (50) Gaus, M.; Goez, A.; Elstner, M. Parametrization and Benchmark of DFTB3 for Organic Molecules. *J. Chem. Theory Comput.* **2013**, *9* (1), 338–354.
- (51) Terekhov, S. S.; Mokrushina, Y. A.; Nazarov, A. S.; Zlobin, A.; Zalevsky, A.; Bourenkov, G.; Golovin, A.; Belogurov, A., Jr; Osterman, I. A.; Kulikova, A. A.; Mitkevich, V. A.; Lou, H. J.; Turk, B. E.; Wilmanns, M.; Smirnov, I. V.; Altman, S.; Gabibov, A. G. A Kinase Bioscavenger Provides Antibiotic Resistance by Extremely Tight Substrate Binding. *Sci Adv* **2020**, *6* (26), eaaz9861.
- (52) Zlobin, A.; Golovin, A. Between Protein Fold and Nucleophile Identity: Multiscale Modeling of the TEV Protease Enzyme-Substrate Complex. *ACS Omega* **2022**, *7* (44), 40279–40292.
- (53) Zlobin, A. S.; Zalevsky, A. O.; Mokrushina, Y. A.; Kartseva, O. V.; Golovin, A. V.; Smirnov, I. V. The Preferable Binding Pose of Canonical Butyrylcholinesterase Substrates Is Unproductive for Echothiophate. *Acta Naturae* **2018**, *10* (4), 121–124.
- (54) Mokrushina, Y. A.; Golovin, A. V.; Smirnov, I. V.; Chatziefthimiou, S. D.; Stepanova, A. V.; Bobik, T. V.; Zalevsky, A. O.; Zlobin, A. S.; Kononov, K. A.; Terekhov, S. S.; Stepanov, A. V.; Papiya, S. O.; Shamborant, O. G.; Round, E.; Belogurov, A. A., Jr; Bourenkov, G.; Makarov, A. A.; Wilmanns, M.; Xie, J.; Blackburn, G. M.; Gabibov, A. G.; Lerner, R. A. Multiscale Computation Delivers Organophosphorus Reactivity and Stereoselectivity to Immunoglobulin Scavengers. *Proc. Natl. Acad. Sci. U. S. A.* **2020**, *117* (37), 22841–22848.
- (55) Caldeweyher, E.; Ehlert, S.; Hansen, A.; Neugebauer, H.; Spicher, S.; Bannwarth, C.; Grimme, S. A Generally Applicable Atomic-Charge Dependent London Dispersion Correction. *J. Chem. Phys.* **2019**, *150* (15), 154122.
- (56) Barducci, A.; Bussi, G.; Parrinello, M. Well-Tempered Metadynamics: A Smoothly Converging and Tunable Free-Energy Method. *Phys. Rev. Lett.* **2008**, *100* (2), 020603.
- (57) Tiwary, P.; Parrinello, M. A Time-Independent Free Energy Estimator for Metadynamics. *J. Phys. Chem. B* **2015**, *119* (3), 736–742.